

JUL 1976  
RECEIVED  
NASA STI FACILITY  
INPUT BRANCH

(NASA-CR-149920) THERMAL AND CONVECTION  
ANALYSES OF THE DENIRITE REMELTING ROCKET  
EXPERIMENT; EXPERIMENT 74-21 IN THE SPACE  
PROCESSING ROCKET PROGRAM Final Report  
(Lockheed Missiles and Space Co.) 50 p

N76-27285

HC \$4.00

Unclas

63/12 44517

*Lockheed*

Missiles & Space Company, Inc.

**HUNTSVILLE RESEARCH & ENGINEERING CENTER**

---

Cummings Research Park  
4800 Bradford Drive,  
Huntsville, Alabama

THERMAL AND CONVECTION  
ANALYSES OF THE DENDRITE  
REMELTING ROCKET  
EXPERIMENT;  
EXPERIMENT 74-21  
IN THE SPACE PROCESSING  
ROCKET PROGRAM  
FINAL REPORT

31 May 1976

Contract NAS8-31800

Prepared for National Aeronautics and Space Administration  
Marshall Space Flight Center, Alabama 35812

by

P. G. Grodzka  
J. E. Pond  
L. W. Spradley

APPROVED:

*J. W. Benefield*  
\_\_\_\_\_  
J. W. Benefield, Supervisor  
Advanced Technology Systems Section

*J. S. Farrior*  
\_\_\_\_\_  
J. S. Farrior  
Resident Director

## FOREWORD

This document reports the results of a four-month study conducted by personnel of the Lockheed-Huntsville Research & Engineering Center under Contract NAS8-31800 and entitled "Experiment 74-21 Space Processing Rocket Program" for NASA-Marshall Space Flight Center. The stated contract requirements are:

- A. Provide analytical support for fluid flow phenomena in Sounding Rocket Experiment 74-21.
- B. Evaluate the extent of fluid flow in Experiment 74-21 under ground-based and sounding rocket flight conditions.

The NASA contract monitor for this investigation was Ms. Carolyn Griner of the MSFC Materials and Processes Laboratory (M&PL). Dr. May Helen Johnson of MSFC/M&PL served as Principal Investigator for Experiment 74-21.

CONTENTS

Section	Page
FOREWORD	ii
1 INTRODUCTION AND SUMMARY	1
2 EXPERIMENT DESCRIPTION	2
3 THERMAL ANALYSIS	13
4 CONVECTION ANALYSIS	17
5 DISCUSSION	33
6 CONCLUSIONS	37
REFERENCES	38
Appendix	
Dynamic and Thermodynamic Similitude of Ground and Flight Experiments	A-1

## 1. INTRODUCTION AND SUMMARY

The Dendrite Remelting Rocket Experiment (Experiment 74-21) was performed aboard a Black Brandt VC Sounding Rocket during a period which gravity levels of approximately  $10^{-5}$  g prevailed. The experiment consisted of cooling an aqueous ammonium chloride solution in a manner such that crystallization of ammonium chloride crystals proceeded throughout a three minute period of "zero-g." The crystallization process during flight was recorded on 35 mm panatomic-x film. A number of ground crystallizations were similarly recorded for comparison purposes.

The purpose of the present study was to assess the convective and thermal conditions in aqueous and metallic liquid systems under conditions of the flight experiment to help establish the relevance of the rocket experiment to metals casting phenomena. The results of the study indicate that aqueous or metallic convective velocities in the Dendrite Remelting Rocket Experiment cell are of insignificant magnitudes at the  $10^{-4}$  to  $10^{-5}$  g levels of the experiment. The crystallization phenomena observed in the Rocket Experiment, therefore, may be indicative of how metals will solidify in low-g. The influence of possibly differing thermal fields, however, remains to be assessed. The Rocket Experiment may also be relevant to how metals solidify on the ground at temperature differences and in cell configurations such that the flow velocities are not high enough to break or bend delicate dendrite arms. Again, however, the influence of the nature of the thermal fields must be assessed. The possible influence of a dissimilar solute boundary layer also must be assessed. Computer calculations of metallic convection at one-g level, while possible, involve complications that were beyond the scope of the present study to address. The complications are discussed in the Convection Analysis Section. Considerations relevant to identifying the conditions whereby a given fluid flow pattern of a given velocity and temperature distribution in ammonium chloride could be matched in a molten metal system are presented in an appendix.

## 2. EXPERIMENT DESCRIPTION

The experiment description given here is brief and limited only to those aspects that are of interest in the present study. The experiment cell had the geometry and dimensions shown in Fig. 1.

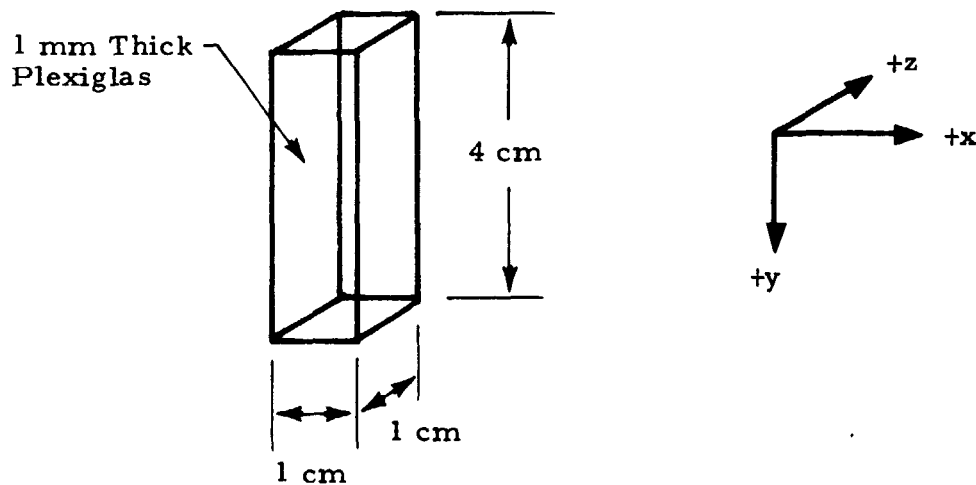


Fig. 1 - Experiment Cell Geometry, Dimensions and Gravity Coordinates During Flight

The coordinates shown in Fig. 1 are the designated gravity vectors during the rocket flight. A record of the gravity levels in the designated directions during the flight are shown in Figs. 2, 3 and 4. Note that y direction experienced the highest levels - about  $2.5 \times 10^{-5}$  g.

The experiment cell was cooled by thermoelectric devices on two sides and the crystal growth viewed through two other sides. The cooling and viewing arrangements are shown in Fig. 5.

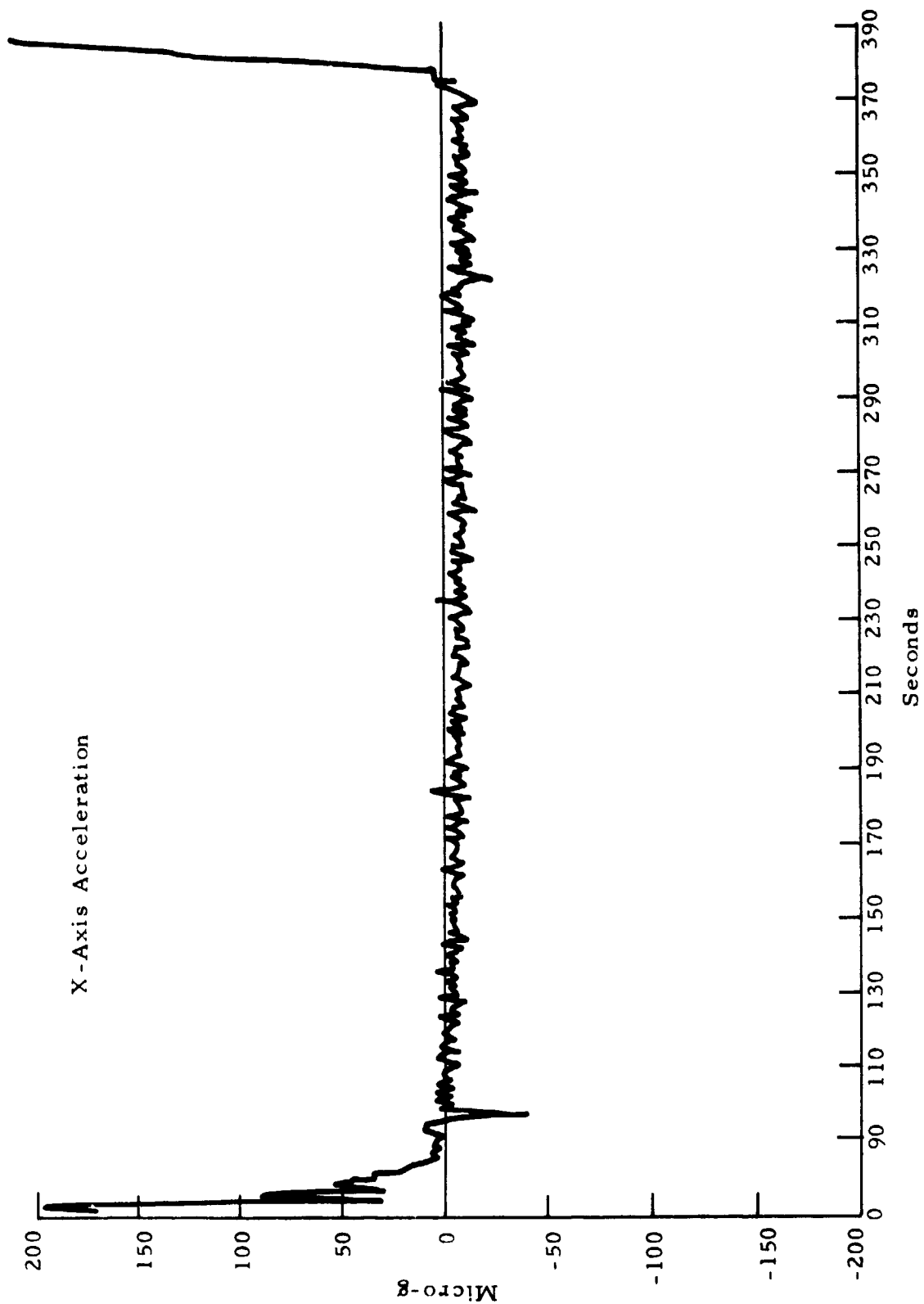


Fig. 2 - Gravity in X-Direction During Flight Test

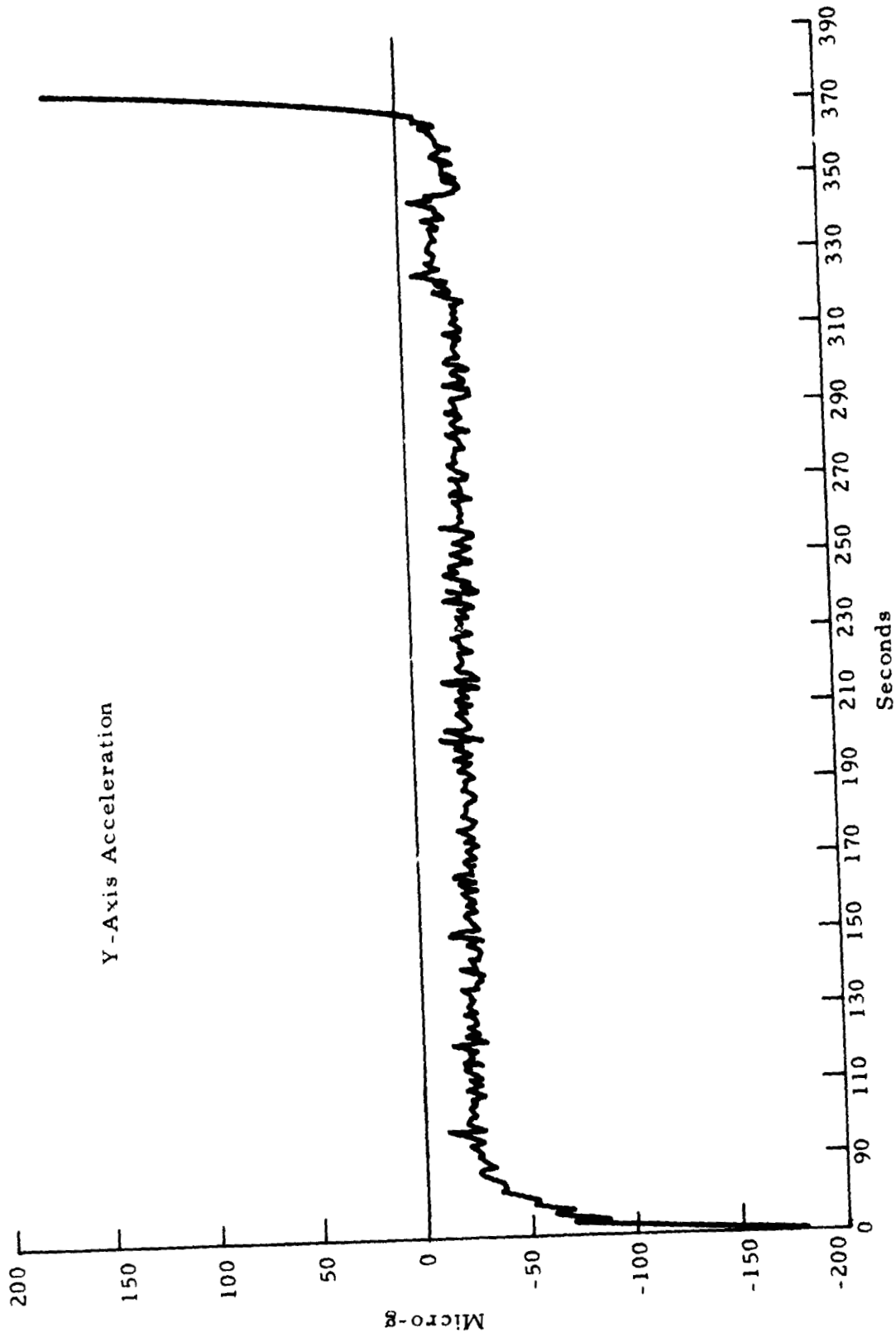


Fig. 3 - Gravity in Y-Direction During Flight Test



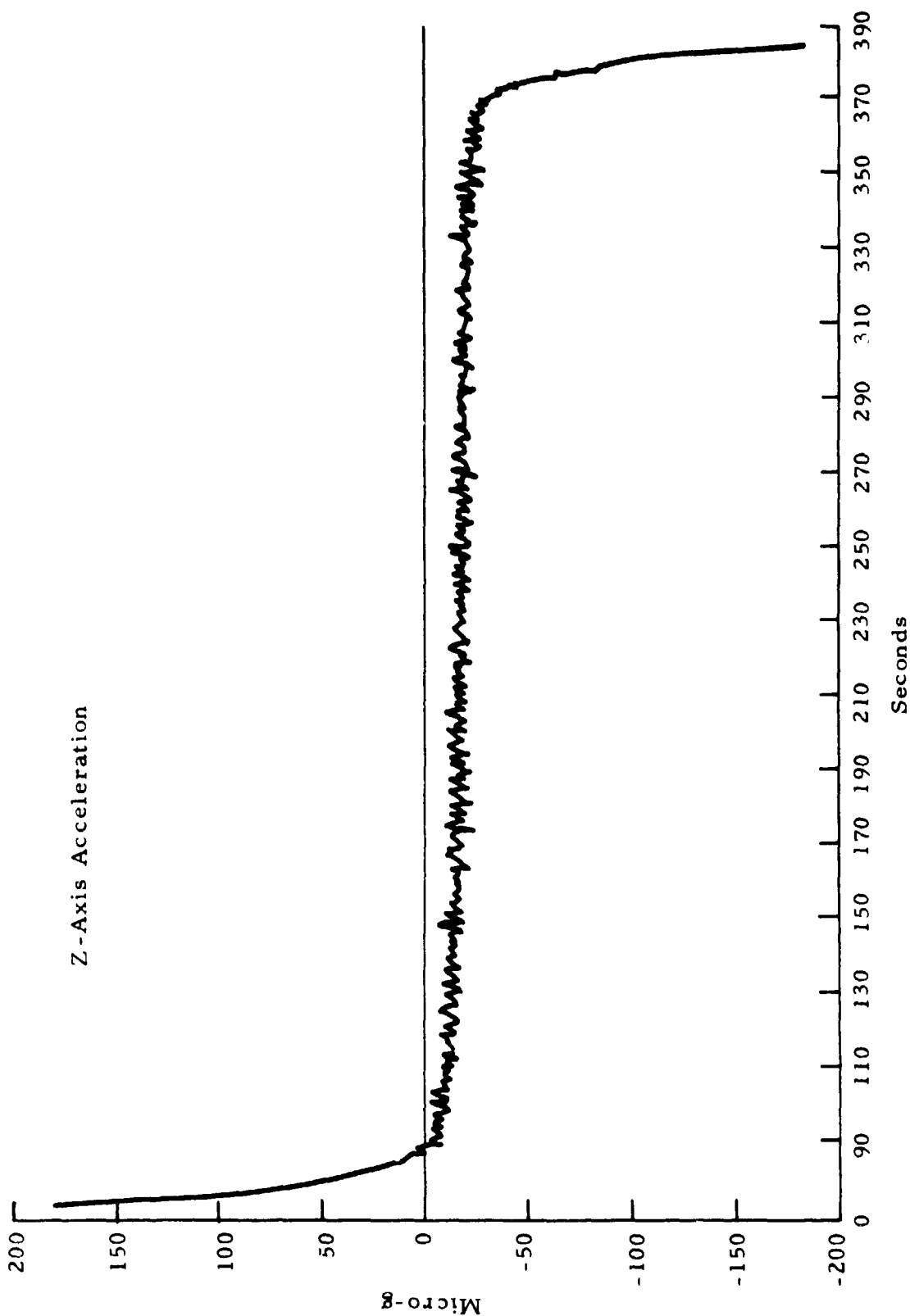


Fig. 4 - Gravity in Z-Direction During Flight Test

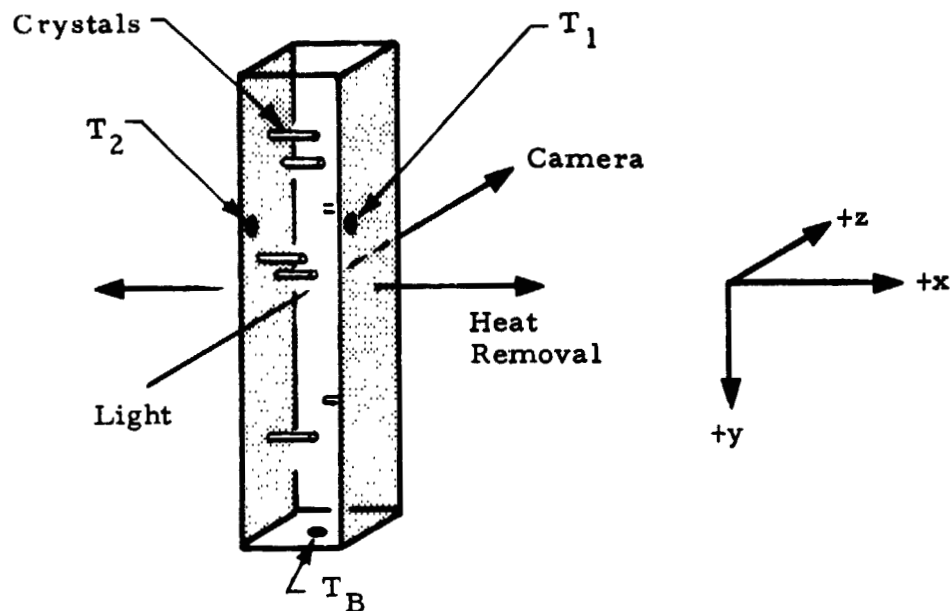


Fig. 5 - Cooling and Viewing Arrangements of Experiment

Two thermistors,  $T_1$  and  $T_2$ , were located at the two cooled walls and one at the bottom of the cell as shown in Fig. 5. Thermistor  $T_B$  was separated from the cell wall by  $2\frac{1}{2}$  mm of plexiglas. The temperature data from thermistor B was not utilized in this study but is included for completeness. Assumptions used in this study were that the cooled walls were cooled uniformly and the thermistor data accurately reflects the outside wall temperature.

Ground tests were conducted with the cell in two positions with respect to the earth gravity vector. The two ground positions are shown in Fig. 6.

The flight and ground test temperature data are given in Table 1.

Figure 7 shows how the external temperature,  $T_1$ , varied in the flight test and in the ground-vertical test as a function of time. It can be seen that although the rate of temperature change was about the same in the two

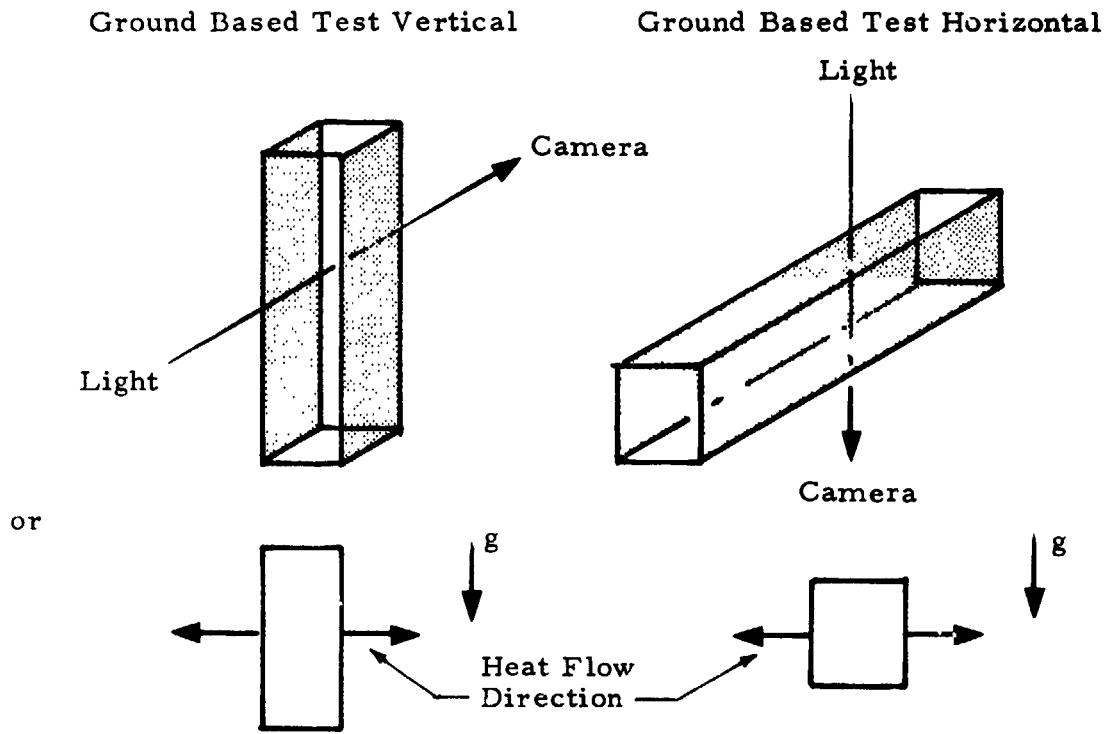


Fig. 6 - Orientations of Test Cell During Ground Tests

Table 1  
OBSERVED TEMPERATURES DURING FLIGHT AND GROUND TESTS

Flight Case Time (sec) (t = 0, time cooling began or 60 sec after liftoff)	Temperature (C)		
	T <sub>B</sub>	T <sub>1</sub>	T <sub>2</sub>
0	24.0	23.8	23.5
5	24.0	23.5	23.8
10	24.0	22.9	22.7
15	24.0	21.3	19.7
20	23.5	20.5	17.2
25	23.6	17.4	15.0
30	24.0	15.3	12.3
35	24.0	15.0	11.6
40	23.6	12.2	9.5
45	24.1	11.0	7.8
50	23.8	9.7	6.0
55	23.5	8.5	4.7
60	23.3	6.8	3.5
65	23.3	6.0	2.0
70	22.9	5.3	1.0
75	22.7	3.7	0.9
80	22.6	2.7	0.2
85	22.2	2.6	-0.3
90	22.0	2.0	-1.3
95	21.8	1.8	-2.2
100	21.5	1.5	-2.3
105	21.1	0.5	-2.3
110	20.7	-0.5	-3.4
115	20.4	-0.5	-4.0
120	20.4	-0.6	-4.1
125	20.0	-2.0	-4.2
130	19.9	-2.2	-4.2
135	19.0	-2.3	-5.5
140	18.7	-2.7	-5.7
145	18.3	-2.8	-6.0
150	17.7	-2.8	-6.0
155	17.3	-4.0	-6.3
160	16.8	-4.2	-6.8
165	16.5	-4.2	-7.0
170	16.1	-4.6	-7.2
175	16.1	-4.6	-7.2

Table 1 (Continued)

Time (sec)	Temperature (C)		
	T <sub>B</sub>	T <sub>1</sub>	T <sub>2</sub>
180	15.5	-4.7	-7.2
185	15.0	-4.7	-8.0
190	14.6	-5.0	-8.2
195	14.3	-5.1	-8.5
200	13.7	-6.0	-8.5
205	13.6	-5.8	-8.5
210	13.5	-6.0	-8.2
215	13.4		-8.5
220	12.9	-5.8	-8.8
225	12.5	-6.3	-8.8
230	12.4	-6.6	-9.3
235	12.2	-6.6	-9.3
240	11.7	-6.8	-9.2
245	11.5	-7.0	-9.5
250	11.4		-9.5
255	11.3	-7.0	-9.5
260	10.8	-7.0	-9.5
265	10.9	-7.5	-9.5
270	10.8	-7.3	-9.5
275	10.4	-7.0	-9.5
280	10.3	-6.8	-9.5
285	10.3	-7.3	-9.5
290	10.3	-6.8	-9.5
295	10.2	-7.5	-9.5
300	10.1	-7.3	-9.2
<u>Ground Base Test - Vertical</u>			
0	23.1	21.7	22.5
30	23.1	11.9	12.8
60	21.9	6.39	7.22
90	19.7	3.06	3.61
120	17.2	1.11	0.833
150	14.4	0	-0.556
180	12.5	-1.11	-1.39
210	10.0	-1.67	-2.78
240	8.61	-2.22	-3.06
270	7.50	-2.77	-3.61
300	6.94	-3.05	-4.444

Table 1 (Concluded)

Ground Base Test -- Horizontal

Time (sec)	Temperature (C)		
	T <sub>B</sub>	T <sub>1</sub>	T <sub>2</sub>
0	18.6	18.6	16.1
30	18.6	7.2	7.2
60	17.8	0.0	0.0
90	16.7	-2.2	-2.2
120	15.0	-3.6	-4.4
150	13.2	-4.4	-5.6
180	11.4	-5.0	-6.1
210	9.72	-5.3	-6.7
240	8.06	-5.6	-6.7
270	6.94	-5.6	-7.7
300	5.56	-5.8	-7.5

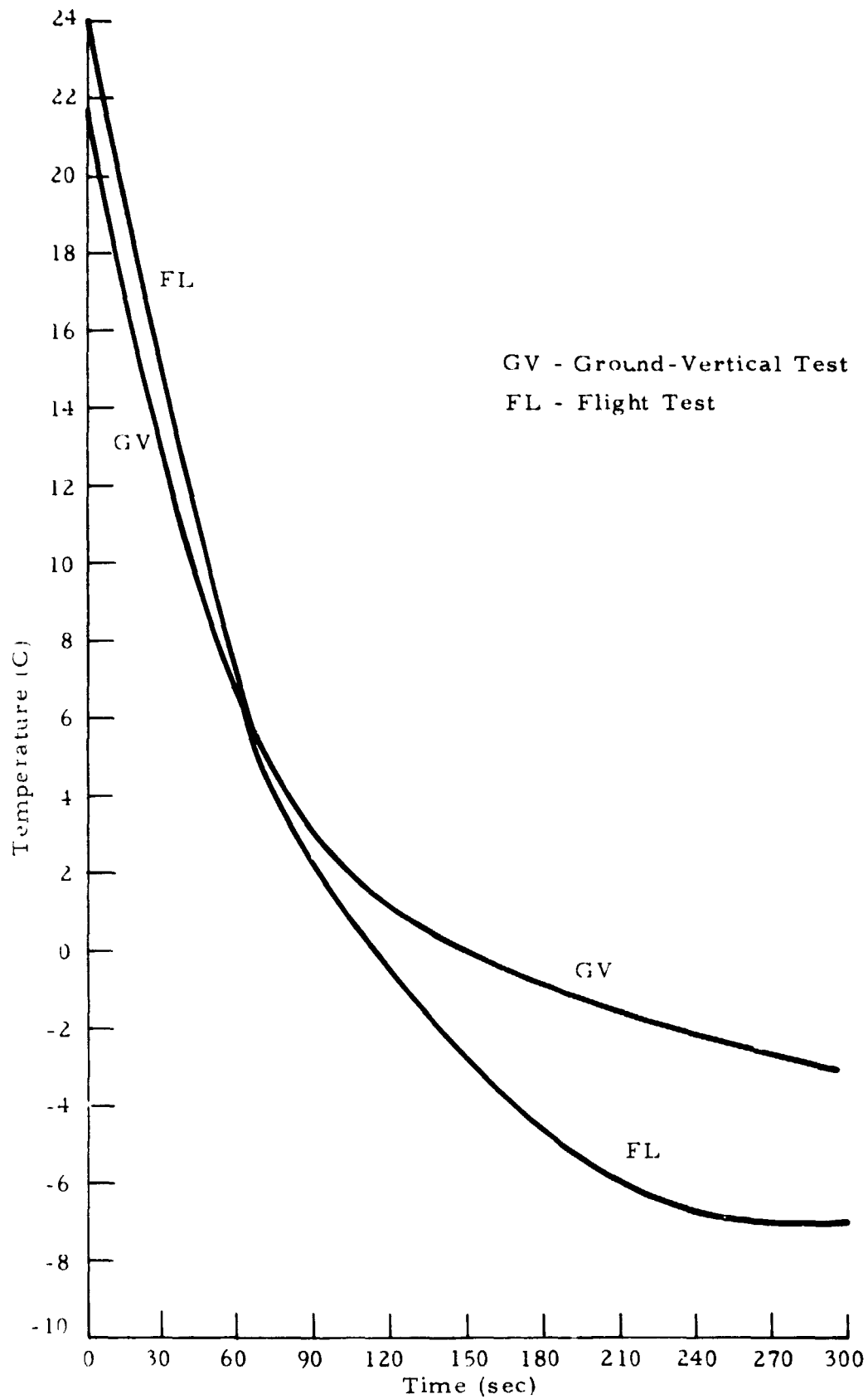


Fig. 7 - Comparison of Time-Temperature Curves for Temperature  $T_1$  in Flight and Ground-Vertical Tests

cases for about 60 sec, thereafter a marked deviation occurred. The higher ground temperatures after 60 sec were primarily the result of vigorous convection in the liquid. The point is discussed in more detail in the Discussion Section.

The times at which nucleation was observed in the ground and flight tests is as follows:

	Inner $T_1$ Wall or $T'_1$	Inner $T_2$ Wall or $T'_2$
Ground Tests		51 sec
Flight Test	109 sec	63 sec
		109 sec



### 3. THERMAL ANALYSIS

Temperatures within the cell as the result of conduction only, where  $g = 0$ , were obtained from computer calculations. The cell was modeled according to the schematic shown in Fig. 8.

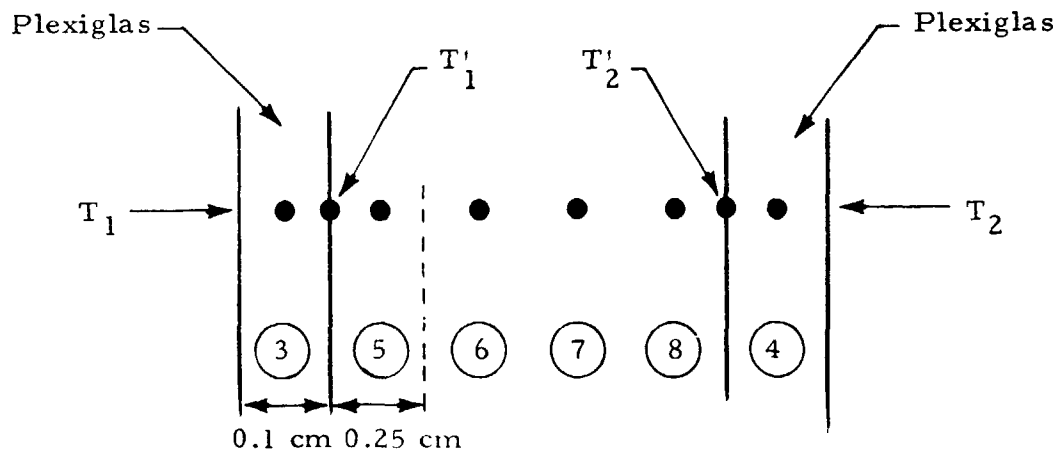


Fig. 8 - Computer Model for Thermal Conduction Analysis

The numbers in the circles are nodes, i.e., the points between which the computer calculates the temperature. Calculated time-temperature values at the designated nodes are given in Table 2. The thermal diffusivity used for Plexiglas was  $1.09 \times 10^{-3} \text{ cm}^2/\text{sec}$  and  $1.51 \times 10^{-3} \text{ cm}^2/\text{sec}$  for the ammonium chloride solution. The conduction temperature profiles in the liquid are generally as shown in Fig. 9. Figure 10 shows temperatures at selected nodes as a function of time from initiation of cooldown.

These temperatures are required for the convection analysis (Section 4) and the crystallization analysis (Section 5).

Table 2  
 CALCULATED INTERNAL TEMPERATURES OF SOLUTION ASSUMING CONDUCTION  
 AS ONLY TRANSPORT MECHANISM (ALL TEMPERATURES IN CENTIGRADE DEGREES)

Time After Cooling Initiation (sec)	Observed External Wall Temperatures		Nodes						Calculated Inner Wall Temp.	
	T <sub>1</sub>	T <sub>2</sub>	3	4	5	6	7	8	T' <sub>1</sub>	T' <sub>2</sub>
0	23.8	23.5	23.7	23.7	23.7	23.7	23.7	23.7	23.7	23.7
5	23.5	23.8	23.7	23.7	23.7	23.7	23.7	23.7	23.7	23.7
10	22.9	22.7	23.4	23.4	23.7	23.7	23.7	23.7	23.4	23.5
15	21.3	19.7	22.6	22.0	23.7	23.7	23.7	23.7	22.7	22.2
20	20.5	17.2	21.5	19.7	23.6	23.7	23.7	23.6	21.7	20.1
25	17.9	15.0	20.1	17.5	23.6	23.7	23.7	23.5	20.5	18.1
30	15.3	12.3	18.0	15.3	23.5	23.7	23.7	23.4	18.5	16.1
35	15.0	11.6	16.3	13.5	23.4	23.7	23.7	23.2	17.0	14.4
40	12.2	9.0	15.0	12.0	23.2	23.7	23.7	23.0	15.8	13.1
45	11.0	7.8	13.2	10.2	23.0	23.7	23.7	22.8	14.1	11.4
50	9.7	8.8	11.9	8.8	22.8	23.7	23.7	22.5	12.9	10.1
55	8.5	4.7	10.7	7.3	22.6	23.7	23.7	22.2	11.8	8.8
60	6.8	3.5	9.4	6.1	22.3	23.6	23.6	21.9	10.7	7.6
65	6.0	2.0	8.2	4.8	22.1	23.6	23.6	21.6	9.5	6.5
70	5.3	1.0	7.3	3.6	21.8	23.6	23.6	21.2	8.7	5.3
75	3.7	9.0	6.4	2.9	21.5	23.6	23.6	20.9	7.8	4.6
80	2.7	0.2	5.2	2.5	21.2	23.6	23.5	20.5	6.7	4.2
85	2.6	-0.3	4.5	1.9	20.9	23.5	23.5	20.2	6.0	3.7
90	2.0	-1.3	4.1	1.3	20.5	23.5	23.4	19.8	5.7	3.1
95	1.8	-2.2	3.6	0.4	20.2	23.5	23.4	19.4	5.2	2.2
100	1.5	-2.3	3.4	-0.2	19.9	23.4	23.3	19.1	5.0	1.7
105	0.5	-2.3	2.9	-0.4	19.6	23.3	23.3	18.7	4.5	1.5
110	-0.5	-3.4	2.0	-0.8	19.3	23.3	23.2	18.3	3.7	1.1
115	-0.5	-4.0	1.4	-0.2	18.9	23.3	23.2	18.0	3.1	0.3
120	-0.6	-4.1	1.2	-2.0	18.6	23.2	23.1	17.6	2.9	-0.1
125	-2.0	-4.2	0.7	-2.2	18.3	23.2	23.1	17.3	2.4	-0.3
130	-2.2	-4.2	-0.1	-2.3	18.0	23.1	23.0	16.9	1.6	-0.5
135	-2.3	-5.5	-0.4	-2.7	17.6	23.0	22.9	16.6	1.3	-0.9
140	-2.7	-5.7	-0.6	-3.5	17.3	23.0	22.8	16.2	1.1	-1.6
145	-2.8	-6.0	-0.9	-3.8	17.0	22.9	22.8	15.9	0.8	-1.9
150	-2.8	-6.0	-1.0	-4.0	16.7	22.8	22.7	15.5	0.7	-2.1
155	-4.0	-6.3	-1.5	-4.2	16.4	22.8	22.6	15.7	0.3	-2.3
160	-4.2	-6.8	-2.1	-4.5	16.0	22.7	22.5	14.9	-0.4	-2.7
165	-4.2	-7.0	-2.4	-4.9	15.7	22.6	22.4	14.5	-0.6	-3.0
170	-4.6	-7.2	-2.6	-5.1	15.4	22.5	22.3	14.2	-0.8	-3.3
175	-4.6	-7.2	-2.8	-5.3	15.1	22.4	22.2	13.9	-1.1	-3.4
180	-1.7	-7.2	-2.9	-5.3	14.8	22.3	22.1	13.6	-1.2	-3.5
185	-4.7	-8.0	-3.0	-5.6	14.5	22.2	22.0	13.3	-1.3	-3.8
190	-5.0	-8.2	-3.1	-6.1	14.2	22.1	21.9	13.0	-1.4	-4.3
195	-5.1	-8.5	-3.3	-6.4	14.0	22.0	21.8	12.7	-1.6	-4.6
200	-6.6	-8.5	-3.7	-6.6	13.7	21.9	21.7	12.3	-2.0	-4.8
205	-5.8	-8.5	-4.1	-6.7	13.4	21.8	21.6	12.1	-2.4	-4.9
210	-6.0	-8.2	-4.2	-6.6	13.1	21.7	21.5	11.8	-2.5	-4.8
215	-5.9	-8.5	-4.3	-6.6	12.9	21.6	21.4	11.5	-2.6	-5.1
220	-5.8	-8.8	-4.2	-6.8	12.6	21.5	21.3	11.2	-2.6	-5.3
225	-6.3	-8.8	-4.4	-7.0	12.3	21.4	21.1	11.0	-2.7	-5.5
230	-6.6	-9.3	-4.7	-7.2	12.1	21.3	21.0	10.7	-3.1	-5.8
235	-6.6	-9.3	-4.9	-7.5	11.8	21.1	20.9	10.4	-3.3	-5.8
240	-6.8	-9.2	-5.0	-7.5	11.6	21.1	20.8	10.2	-3.4	-5.9
245	-7.0	-9.5	-5.2	-7.6	11.3	20.9	20.7	9.9	-3.6	-6.1
250	-7.0	-9.5	-5.4	-7.8	11.1	20.8	20.5	9.7	-3.8	-6.1
255	-7.0	-9.5	-5.4	-7.8	10.9	20.1	20.4	9.4	-3.8	-6.2
260	-7.0	-9.5	-5.4	-7.8	10.6	20.6	20.3	9.2	-3.9	-6.2
265	-7.0	-9.5	-5.5	-7.9	10.2	20.3	20.0	8.7	-4.0	-6.3
270	-7.0	-9.5	-5.5	-7.9	10.2	20.3	20.0	8.7	-4.0	-6.3
275	-7.0	-9.5	-5.5	-7.9	10.0	20.2	19.9	8.5	-4.0	-6.3
280	-6.8	-9.5	-5.5	-7.9	9.7	20.0	19.7	8.3	-4.0	-6.4
285	-7.3	-9.5	-5.5	-7.9	9.5	19.9	19.6	8.1	-4.1	-6.4
290	-6.8	-9.5	-5.6	-8.0	9.3	19.8	19.5	7.9	-4.2	-6.4
295	-7.5	-9.5	-5.6	-8.0	9.1	19.7	19.3	7.6	-4.2	-6.5
300	-7.3	-9.2	-5.9	-7.9	8.9	19.6	19.2	7.5	-4.5	-6.4

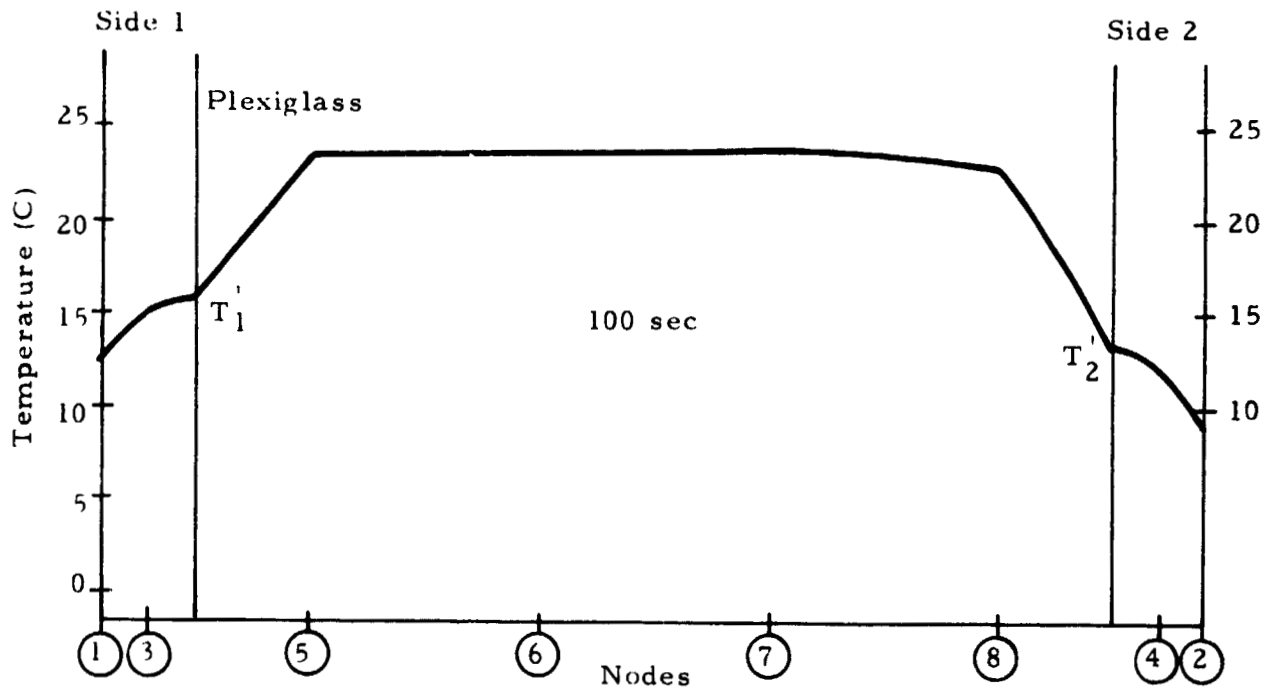
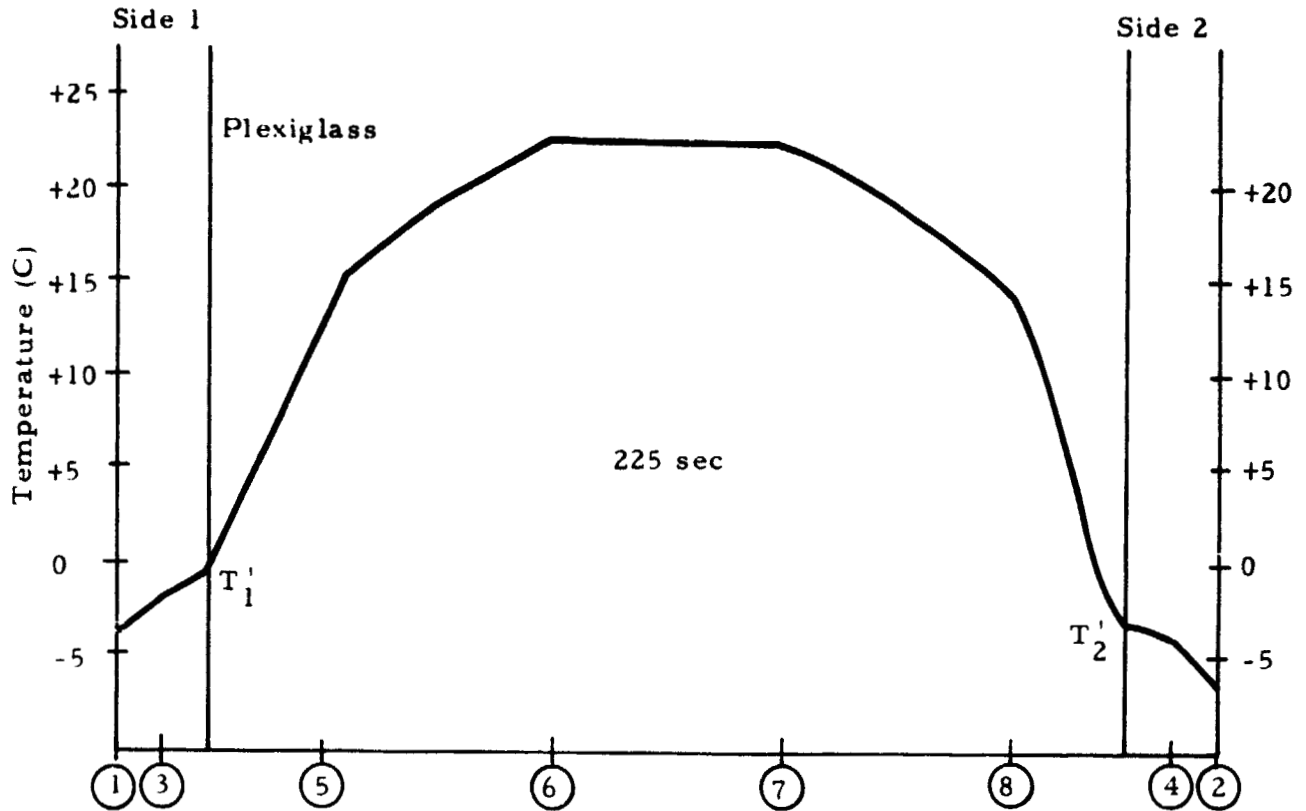


Fig. 9 - Temperature Profile Through 74-21 Experiment Cell, Gravity Equal to Zero

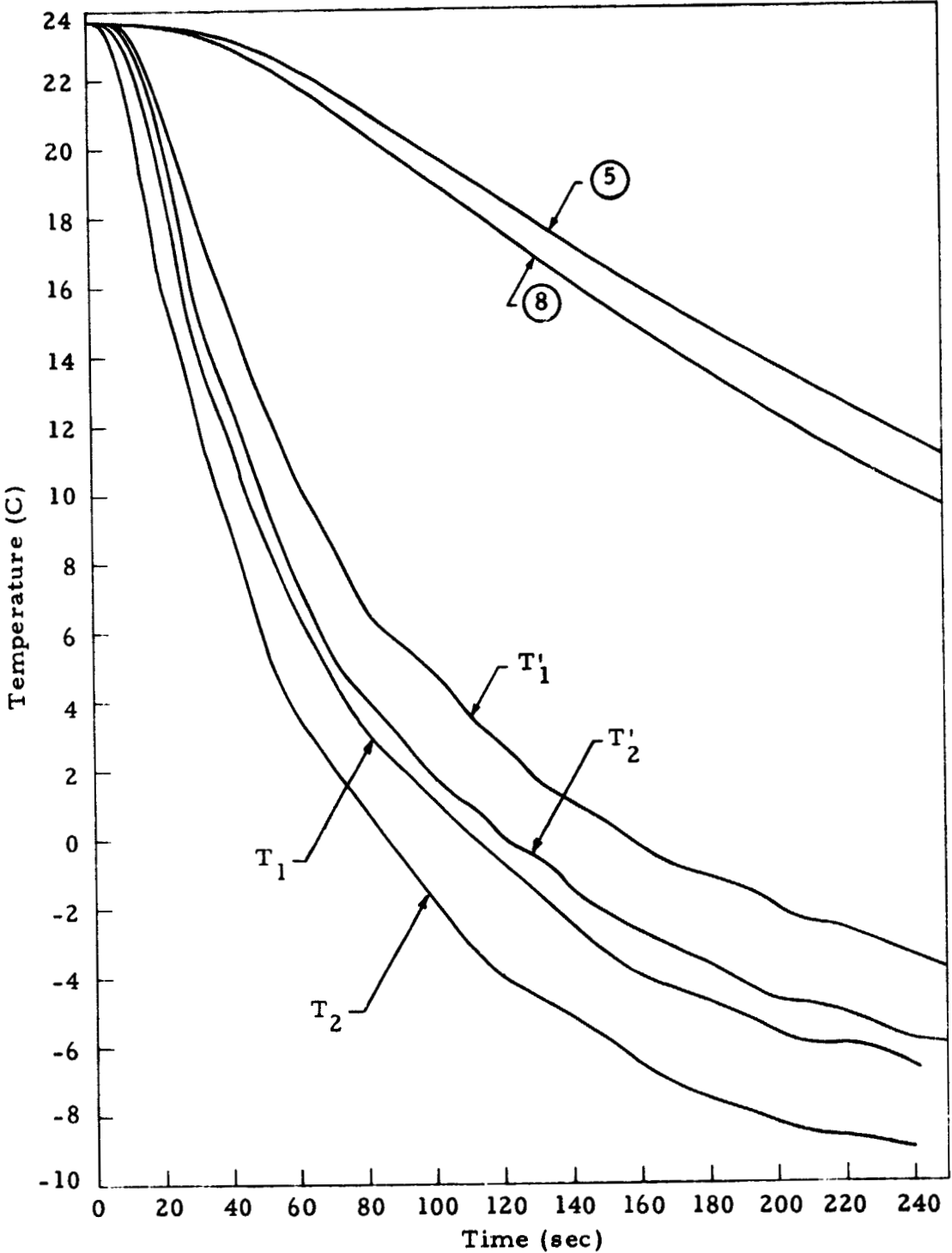


Fig. 10 - Time-Temperature Curves at Selected Conduction Nodes

## 4. CONVECTION ANALYSIS

Dimensionless Analysis: An idea of the types of convection involved and their magnitudes can be gained from a comparison of various dimensionless numbers. The Rayleigh numbers,  $Ra_T$  and  $Ra_S$  are the thermal and solutal Rayleigh numbers, respectively. They are defined by the following equations

$$Ra_T = \frac{g \beta_T \Delta T d^3}{\nu \alpha} \quad Ra_S = \frac{g \beta_C \Delta C d^3}{\nu D_{12}}$$

where  $d$  = distance between hot and cold walls,  $g$  = gravity acceleration,  $\beta_T$  = thermal expansion coefficient,  $\beta_C$  = solute expansion coefficient,  $\Delta T$  = temperature difference between the hot and cold wall,  $\nu$  = kinematic viscosity,  $\alpha$  = thermal diffusivity, and  $D_{12}$  = chemical diffusion coefficient. The Rayleigh numbers are weighed ratios of the buoyancy force to the viscous force and are used to characterize convective flows. For example, when the Rayleigh number exceeds certain critical values, heat flow departs significantly from pure conductive transfer. In cases of heating from below, a critical Rayleigh number defines the point where fluid flow commences. In side heating cases, fluid flow always accompanies any finite temperature gradient so there is no critical Rayleigh number for onset of fluid flow. For the present study these numbers are given in Table 3. Properties used in the calculations of Table 3 are given in Table 4.

Table 3  
COMPARISON OF RAYLEIGH NUMBERS AT ONE-G

System	Conditions	Dimensionless Number
27.8 wt% NH <sub>4</sub> Cl- H <sub>2</sub> O	1 g, $\Delta T = 11$ C, $d = 0.5$ cm	$Ra_T = 3.4 \times 10^4$
	1 g, $\Delta C = 2.4$ wt %, $d = 0.5$ cm	$Ra_S = 4.9 \times 10^6$
80 wt% Pb-Sn	1 g, $\Delta T = 11$ C, $d = 0.5$ cm	$R_T = 591$
	1 g, $\Delta C = 2.4$ wt %, $d = 0.5$ cm	$R_S = 1.5 \times 10^7$

Table 4  
PROPERTY DATA UTILIZED IN CALCULATION OF CASES GIVEN IN TABLE 3

Comparison of Liquid Properties (approximate values)

System	T <sub>m</sub> MP C	μ Viscosity Poise	ν Kinematic Viscosity cm <sup>2</sup> /sec	ρ Density gm/cm <sup>3</sup>	C <sub>p</sub> Specific Heat cal/gm C	k Thermal Conduct. cal/cm-sec C	α Thermal Diffus. cm <sup>2</sup> /sec	Pr $\frac{\mu}{\rho \alpha}$	Sc $\frac{\mu}{D}$	$\frac{\beta_T}{C}$ °C	$\frac{\beta_S}{wt \%}$	D <sub>12</sub> cm <sup>2</sup> /sec	$\frac{1}{\alpha}$	$\frac{1}{D_{12}}$
27.8% NH <sub>4</sub> Cl - H <sub>2</sub> O	23	1 x 10 <sup>-2</sup>	9.3 x 10 <sup>-3</sup>	1.08	0.74	1.204 x 10 <sup>-3</sup>	1.5 x 10 <sup>-3</sup>	6.2	517	2.95 x 10 <sup>-4</sup>	-2.81 x 10 <sup>-3</sup>	1.8 x 10 <sup>-5</sup>	667	5.56 x 10 <sup>4</sup>
80% Pb-Sn	300	2 x 10 <sup>-2</sup>	2 x 10 <sup>-3</sup>	8.5		3.9 x 10 <sup>-2</sup>	0.114		67	1 x 10 <sup>-4</sup>	-3 x 10 <sup>-3</sup>	3 x 10 <sup>-5</sup>	8.77	
20% Pb-In		1.2 x 10 <sup>-2</sup>	1.7 x 10 <sup>-3</sup>	7.82	0.0596	8.8 x 10 <sup>-2</sup>	0.218	.0078		1.38 x 10 <sup>-4</sup>	-3.78 x 10 <sup>-3</sup>			

The relative magnitude of the convective velocities must be determined with detailed computer calculations because no general analytical theory is known that can handle fluids of such high fluidity as metals. For a very rough estimate of the fluid velocities for the two fluid systems under consideration, use of an equation developed by Batchelor for air<sup>(1)</sup> can be used.

Batchelor's equation for the steady-state velocity distribution for air maintained between a constant temperature differential is as follows:

$$u = \frac{r}{12d^2} \alpha R_T \left(1 - \frac{r}{d}\right) \left(1 - \frac{2r}{d}\right) \quad (1)$$

where

$u$  = velocity

$r$  = distance in liquid from sidewalls

$d$  = distance between the two sidewalls

$\alpha$  = thermal diffusivity

$R_T$  = thermal Rayleigh number

Maximum velocities occur at one-quarter distances from the side walls. Very roughly then, maximum velocities can be given by

$$u_{\max} = 0.01 \alpha R_T$$

Similarly

$$u_{\max} = 0.01 D_{12} R_S$$

Utilizing the foregoing relationships the following velocities are obtained for the cases given at the beginning of this section.

System	Driving Force	Estimated Maximum Velocities, cm/sec
27.8% NH <sub>4</sub> Cl · H <sub>2</sub> O	R <sub>T</sub> 3.39 × 10 <sup>4</sup>	0.5
	R <sub>S</sub> 4.9 × 10 <sup>6</sup>	0.9
80% Pb-Sn	R <sub>T</sub> 591	0.7
	R <sub>S</sub> 1.5 × 10 <sup>7</sup>	4.5

On the basis of these figures, it would be expected that solutally driven convection would be much stronger than thermally driven convection and that metal systems should show higher convective velocities than ammonium chloride solutions. The preceding figures are based on steady state theory. The thermal conditions during the rocket flight were not steady state. Thus, the solutal velocities obtained in the computer studies show higher solutal than thermal velocities. The dimensionless numbers that are relevant to estimating how fast maximum convective velocities are attained are the Prandtl, Pr, and Schmidt, Sc, numbers. These are defined as follows:

$$Pr = \frac{\nu}{\alpha} \quad Sc = \frac{\nu}{D_{12}}$$

Table 4 gives values of these numbers for the systems involved. Low values of these numbers mean that the driving forces for convection propagate faster through the liquid than the momentum transfer. Thus higher values of velocity are realized sooner. Because D<sub>12</sub> values are generally quite low, solutally generated convective velocities under the conditions of this study would generally be more slowly attained than thermally generated convective velocities. The preceding discussion illustrates the danger of utilizing dimensionless numbers meant to characterize steady-state convection to obtain information on transient convection.



Another dimensionless number that is of interest in the present study is the stability number,  $Sy$ , which is defined as follows

$$Sy = \frac{Ra_S}{Ra_T} \frac{1}{Le} = \frac{\beta_C \Delta C}{\beta_T \Delta T}$$

where  $Le$  is the Lewis number ( $Le = \frac{\alpha}{D_{12}}$ ).

Lindberg and Haberstrah<sup>(2)</sup> define the following criterion for the onset of a thermal-solutal convection called thermal bursts:

$$Sy < \sqrt{Le}$$

It might be mentioned that a variety of thermal-solutal types of convection are not clearly defined and characterized at present. Fingering, cellular and oscillatory types of convection are possible as the result of the coupled thermal and solutal driving forces. The stability number, therefore, should be viewed only as a diagnostic aid but not as conclusive evidence that thermal-solutal convection does or does not exist in any particular situation. For the ammonium chloride system of the present study the magnitudes of the stability and Lewis numbers are as follows:

$$Sy = 1.8 \quad (\Delta T = 11 \text{ C}, \Delta C = 2.4 \text{ wt } \%)$$

$$Le = 81.1 \quad , \quad \sqrt{Le} = 9$$

Thus, on the basis of the analysis of Lindberg and Haberstrah, thermal bursts could well be expected in the ammonium chloride system of the present study either on the ground or in low-g. Jet-like convections have been previously noted in ammonium chloride systems and have been forwarded as the cause of a defect in metal castings called freckles.<sup>(3)</sup>

A study of thermal-solutal convection in Al-Mg alloys<sup>(4)</sup> predicts a band of liquid at the front of a solidifying interface where convection can occur while the liquid further out is quiescent. Al-Mg alloys are similar to the ammonium chloride system in that the density decreases ahead of the interface as the result of the removal of solute. The value of the band-width,  $x$ , is such that

$$80 \left( \frac{1}{k_o} - 1 \right) \frac{V}{D_{12}} \exp\left(-\frac{Vx}{D_{12}}\right) = \frac{dT}{dx} = G$$

where  $k_o$  is the equilibrium solid-liquid segregation coefficient and  $V$  the velocity of crystallization. Convection occurs when

$$\left( \frac{1}{k_o} - 1 \right) \frac{m}{D_{12}} \cdot \frac{Vx}{D_{12}} = 2.8$$

where  $m$  is the slope of the liquidus line. The topic of thermal-solutal convection is obviously extremely important to metals castings.

Computer Models: With the aid of the Lockheed Convection Analysis Program (LCAP), it is possible to obtain two-dimensional data on internal flow patterns, velocities and temperature, concentration, and density distributions during transient heating or cooling. In the present study LCAP was applied to a variety of problems in connection with the Dendrite Remelting Experiment. The various cases calculated are summarized in Table 5. The boundary conditions for the cases are given in Table 6. Cases for both  $10^{-4}$  g and  $10^{-5}$  g were both calculated for two reasons. First, the g level data while undoubtedly precise may be somewhat in error with regard to accuracy. Apparently some problems exist in calibrating accelerometer data at such low levels. Secondly, because of the small time steps in the computer program required at  $10^{-4}$  g, only a few seconds of real time data were available from the calculations. The  $10^{-4}$  g data, however, was sufficient to ascertain the magnitude of the convective velocities. The  $10^{-5}$  g calculations covered a substantial portion of the

Table 5  
SUMMARY OF CASES CALCULATED BY LCAP CONFIGURATION

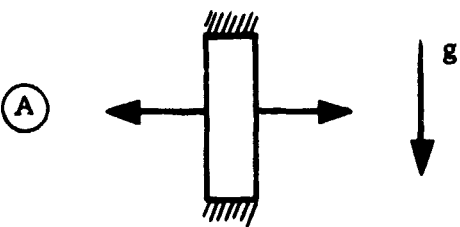
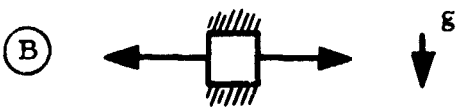
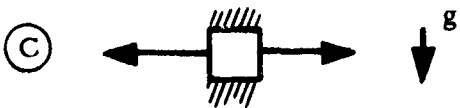
	<ul style="list-style-type: none"> <li>● <math>\text{NH}_4\text{Cl}</math> solution               <ul style="list-style-type: none"> <li><math>g = 1</math>, thermal</li> <li><math>g = 10^{-4}</math>, thermal, solutal</li> <li><math>g = 10^{-5}</math>, thermal, solutal</li> </ul> </li> <li>● 80 wt% Pb-Sn               <ul style="list-style-type: none"> <li><math>g = 10^{-4}</math> and <math>10^{-5}</math>, thermal, solutal</li> </ul> </li> <li>● 20 wt% Pb-In solution               <ul style="list-style-type: none"> <li><math>g = 1</math>, thermal</li> <li><math>g = 10^{-4}</math> and <math>10^{-5}</math>, thermal, solutal</li> </ul> </li> </ul>
	<ul style="list-style-type: none"> <li>● <math>\text{NH}_4\text{Cl}</math> solution               <ul style="list-style-type: none"> <li><math>g = 1</math>, thermal</li> <li><math>g = 10^{-4}</math>, thermal, solutal</li> <li><math>g = 10^{-5}</math>, thermal, solutal</li> </ul> </li> </ul>
	<ul style="list-style-type: none"> <li>● <math>\text{NH}_4\text{Cl}</math> solution               <ul style="list-style-type: none"> <li><math>g = 1, 10^{-4}, \text{ and } 10^{-5}</math>, thermal</li> </ul> </li> </ul> <p>In all of the cases the temperature of the right wall is <math>T_2'</math> and that of the left wall <math>T_1'</math>. Corresponding solute concentrations are <math>C_2'</math> and <math>C_1'</math>.</p>

Table 6  
BOUNDARY CONDITIONS FOR CASES GIVEN IN TABLE 4

NH<sub>4</sub>Cl Solutions at 10<sup>-4</sup> g and 10<sup>-5</sup> g: The temperature T<sub>1</sub>' and T<sub>2</sub>' were obtained from Table 2 for the thermal cases. For the solutal cases the C<sub>1</sub>' and C<sub>2</sub>' terms were obtained from a solubility curve of ammonium chloride as a function of temperature. The actual times and T and C values used are as follows:

Time (sec)	Temp. (C)		Weight (%)	
	T <sub>1</sub> '	T <sub>2</sub> '	C <sub>1</sub> '	C <sub>2</sub> '
0	23.7	23.7	27.8	27.8
30	18.5	16.1	26.8	26.3
60	10.7	7.6	25.0	24.5
90	5.7	3.1	24.0	23.4
120	2.7	0.1	23.4	22.7
150	0.7	-2.1	22.8	22.2
180	-1.2	-3.5	22.4	21.9
210	-2.5	-4.8	22.2	21.6
240	-3.4	-5.8	21.9	21.4
270	-4.0	-6.3	21.8	21.2
300	-4.5	-6.4	21.6	21.1

80 wt % Pb-Sn Solution: About the same thermal and solutal differences were utilized as were applied to low-g NH<sub>4</sub>Cl cases. The initial temperature, however, was 300 C. The conditions used correspond to a realistic case of Pb-Sn solidification.

20% Pb-In: Cases with this system were run to gain insight into how another metallic system would behave and to provide an easy experimental test of some of the conclusions presented here.

(Continued)

Table 6 (Concluded)

Time (sec)	C		Weight (%)	
	T' <sub>1</sub>	T' <sub>2</sub>	C' <sub>1</sub>	C' <sub>2</sub>
0	260	260	20.0	20.0
5	243	243	16.7	16.7
10	226	226	13.3	13.3
15	210	210	10.0	10.0
20	193	193	6.7	6.7
25	176	176	3.3	3.0
30	160	160	0	0
35	160	160		
40	160	160		

NH<sub>4</sub>Cl Solutions at 1 g: The thermal convections at 1 g proved so violent, as is subsequently discussed, that solutal calculations were not pursued. The thermal conditions for the two cases run in the A and B configurations are as follows:

Time (sec)	A Configuration		B Configuration	
	T' <sub>1</sub>	T' <sub>2</sub>	T' <sub>1</sub>	T' <sub>2</sub>
0	21.7	22.5	18.6	16.1
30	15.1	16.1	10.4	11.0

The above values were obtained by adding 3.2 and 3.8 degrees, respectively, to the observed T<sub>1</sub> and T<sub>2</sub> values. The 3.2 and 3.8 values were obtained by subtracting the conduction T'<sub>1</sub> and T'<sub>2</sub> (Table 2) values from the observed T<sub>1</sub> and T<sub>2</sub> flight values, i.e., the 3.2 and 3.8 values represent the corrections to the outer wall temperatures to obtain inner wall temperatures.

time the experiment was conducted and so provided information on transient behavior. In Table 5 the A configuration corresponds to the experimental cell standing upright while the B and C configurations correspond to it lying on its side. The pictorial designations  $\lll$  and  $\rightarrow$  mean insulated wall and direction of heat or solute flow. The term  $\downarrow g$  indicates the direction of the gravity vector. The designations thermal and solutal mean that the calculated convection either arises only from thermally generated buoyancy or only from solutally generated buoyancy. Neither LCAP nor any other known convection program at present can handle coupled thermal-solutal cases for times longer than a few milliseconds. The problem with the coupled calculation is that of the extremely small time steps required to perform the calculation. In order to follow convection for any length of time in coupled cases, unreasonably long calculation periods are required. A great deal of relevant information, however, can still be gained from the uncoupled cases.

The  $10^{-4} g$  and  $10^{-5} g$  ammonium chloride and Pb-In cases show maximum velocities of the orders of magnitude of  $10^{-4}$  to  $10^{-6}$  cm/sec. The Pb-Sn velocities are even lower. Figure 11 shows a couple of typical curves for an ammonium chloride solution case. In all of the low-g cases run, the internal temperature profiles did not deviate to any detectable extent from pure conduction temperature profiles. Figure 12 shows a typical computer picture of an internal temperature profile at a given instant.

The thermal 1 g ammonium chloride shows maximum velocities of 11.6 cm/sec. In reality the ground cases were turbulent. The Pb-In system was run at 1 g. The time step required for a metallic system is so small that only a very small time interval can be calculated in any reasonable length of computer time. The 1 g metallic calculations by computer, therefore, were not pursued further. It may be mentioned, however, that a solution to this problem is available - a new computation technique (alternating direction implicit, ADI) could be introduced into LCAP. Such an alteration of the program would take at least six months.

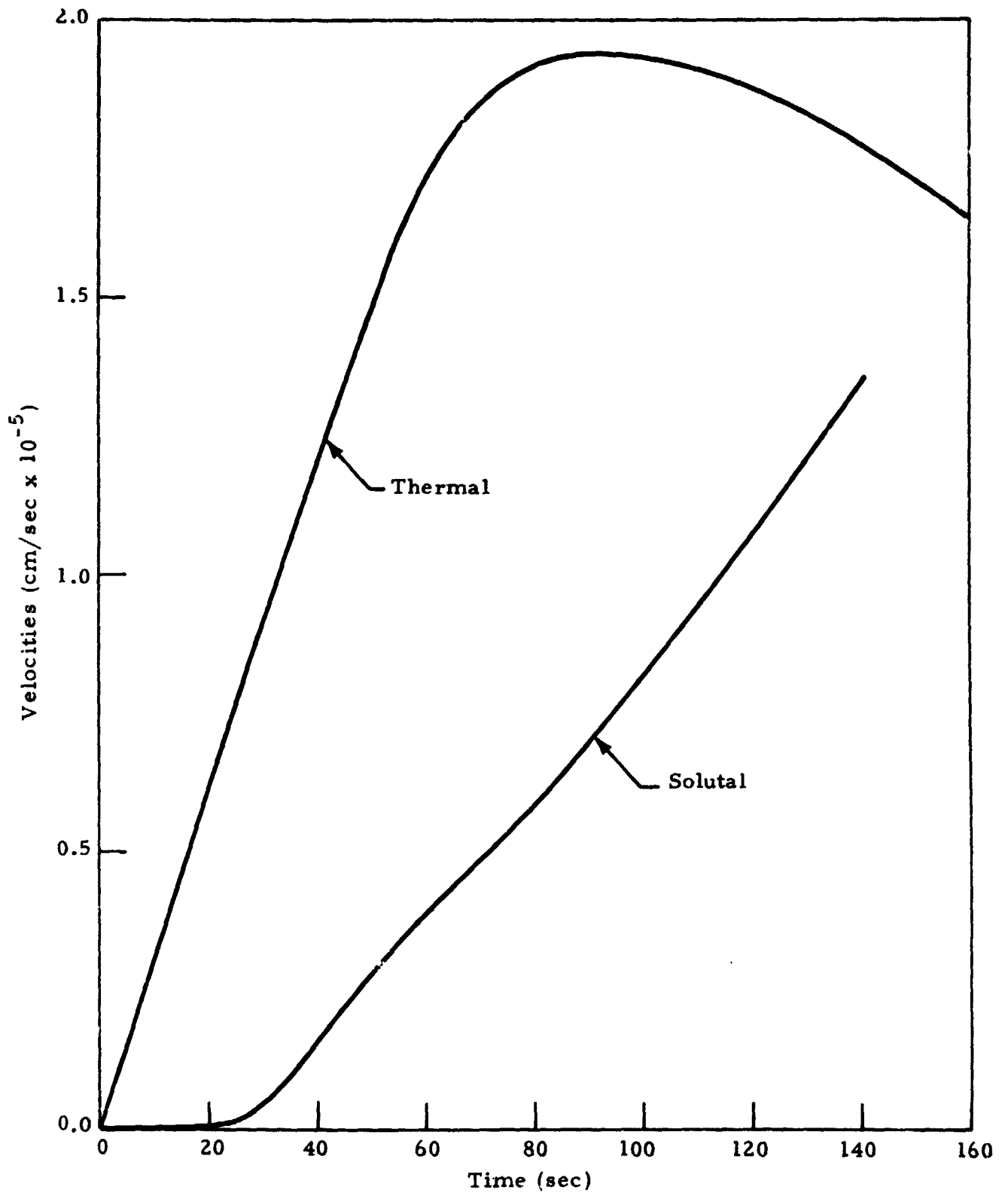


Fig. 11 - Typical Maximum Convective Velocities





Another regrettable feature of not being able to utilize the computer to map convection in metallic systems at 1 g is that the metallic systems at  $10^{-4}$  and  $10^{-5}$  g show significant convective oscillatory behavior. Marked oscillatory behavior at 1 g could be a significant factor in dendrite remelting.

A sample problem was conducted to illustrate the behaviors of transient convection. Figure 13 shows plots of maximum velocity versus time for a thermal and a solutal case in which the driving forces were set by the following condition:

$$\beta_T \Delta T = \beta_C \Delta C$$

i.e., the buoyancy forces are the same in the two cases. The temperature or concentration was dropped at time  $t = 0$  at one wall to a constant lower value. The physical situation, therefore, corresponds to suddenly applying a lower, constant temperature to one wall while the other wall is maintained constant at its initial value. Convection will begin and build up until a steady state is eventually reached. The purpose of the calculation was to see how long it would be before steady state is attained.

LCAP also provides data such as shown in Figs. 14 and 15.

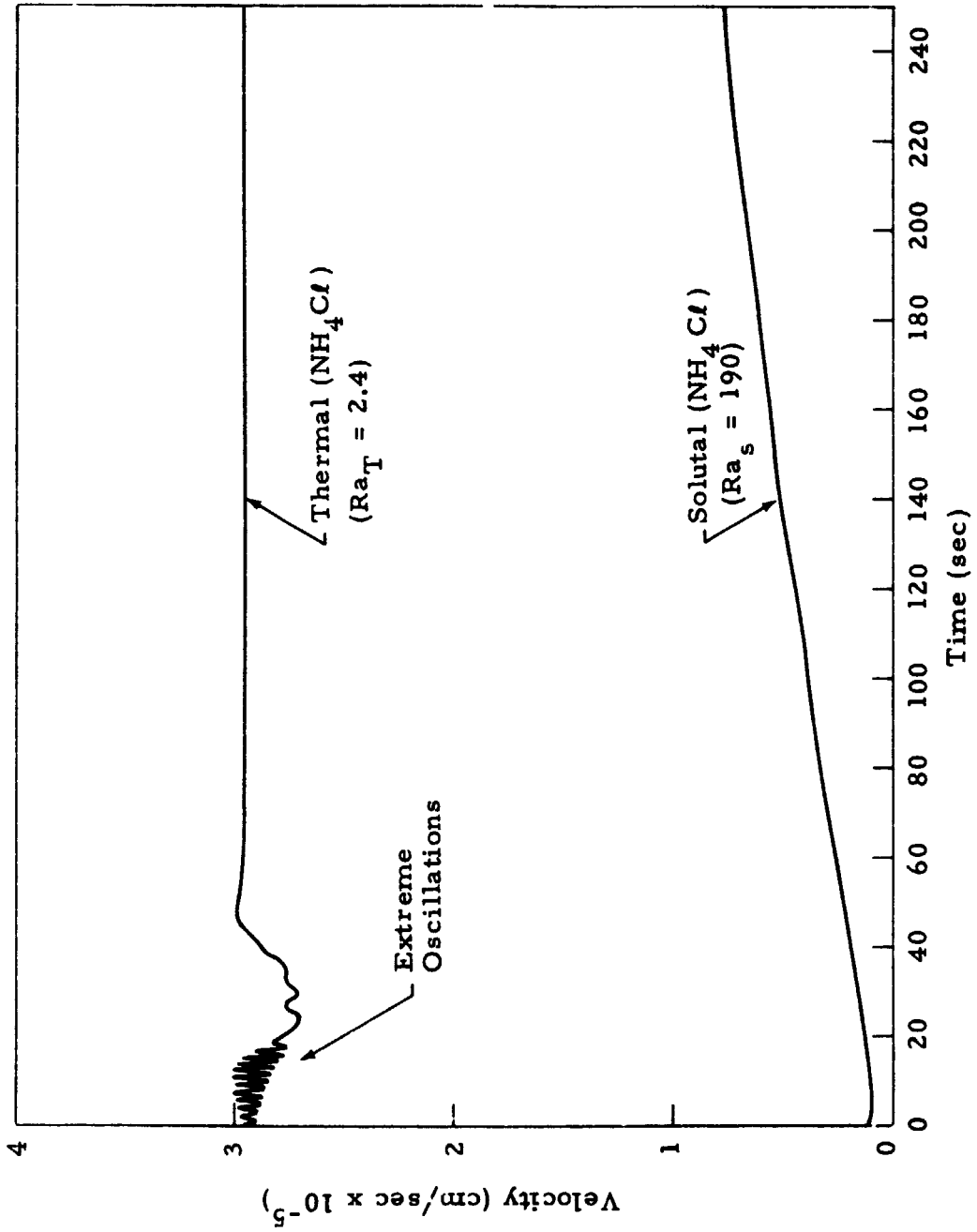


Fig. 13 - Sample Calculation Comparing Convection Development

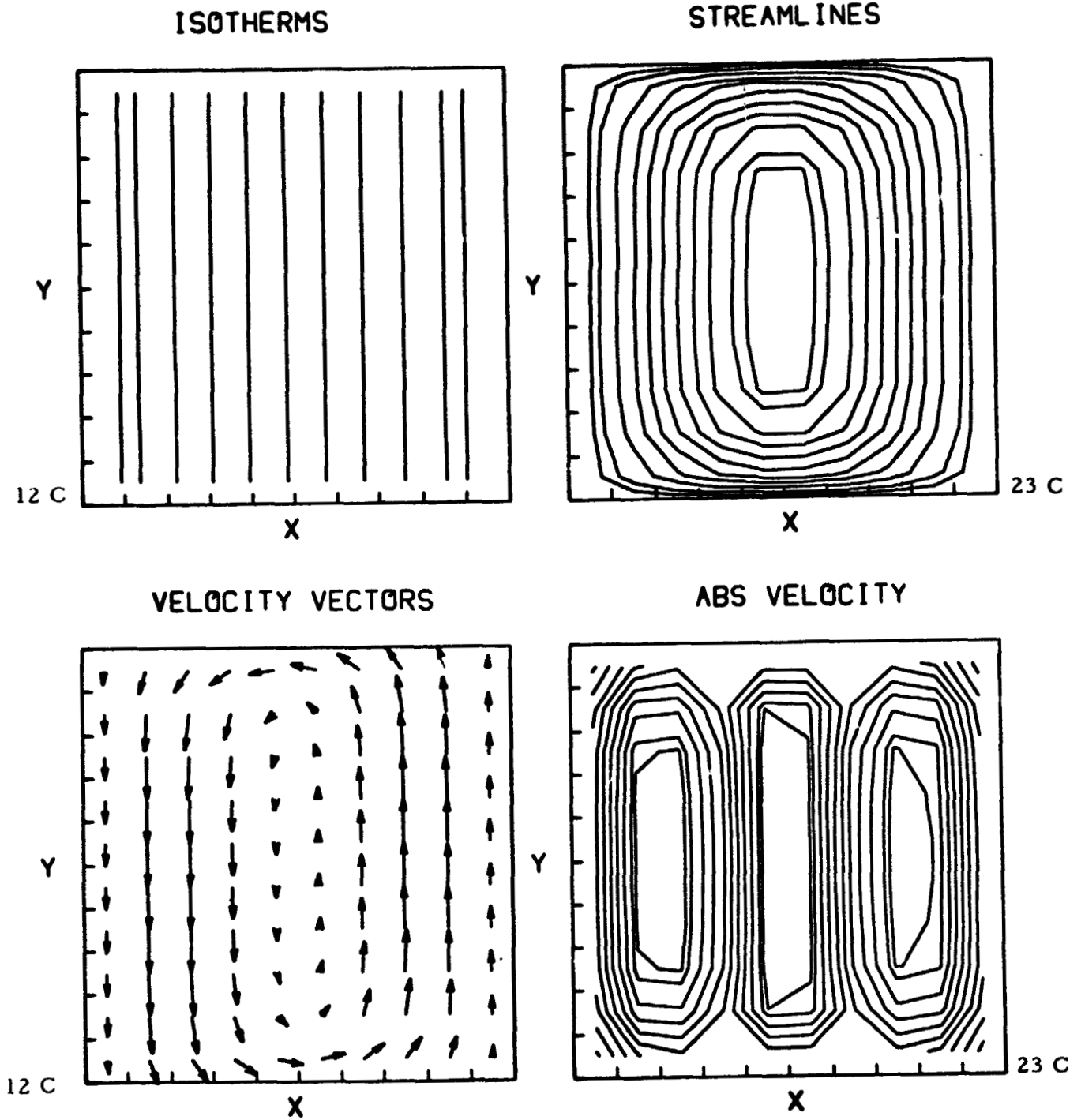


Fig. 14 - LCAP Pictorial Representation of Thermal Convection in Ammonium Chloride Solution at  $10^{-5}g$  (Case is that of the left side temperature being suddenly dropped to 12 C. Length of arrows in the velocity vector plot indicates magnitude of velocity. The ABS or absolute velocity plot shows lines of constant velocity.)

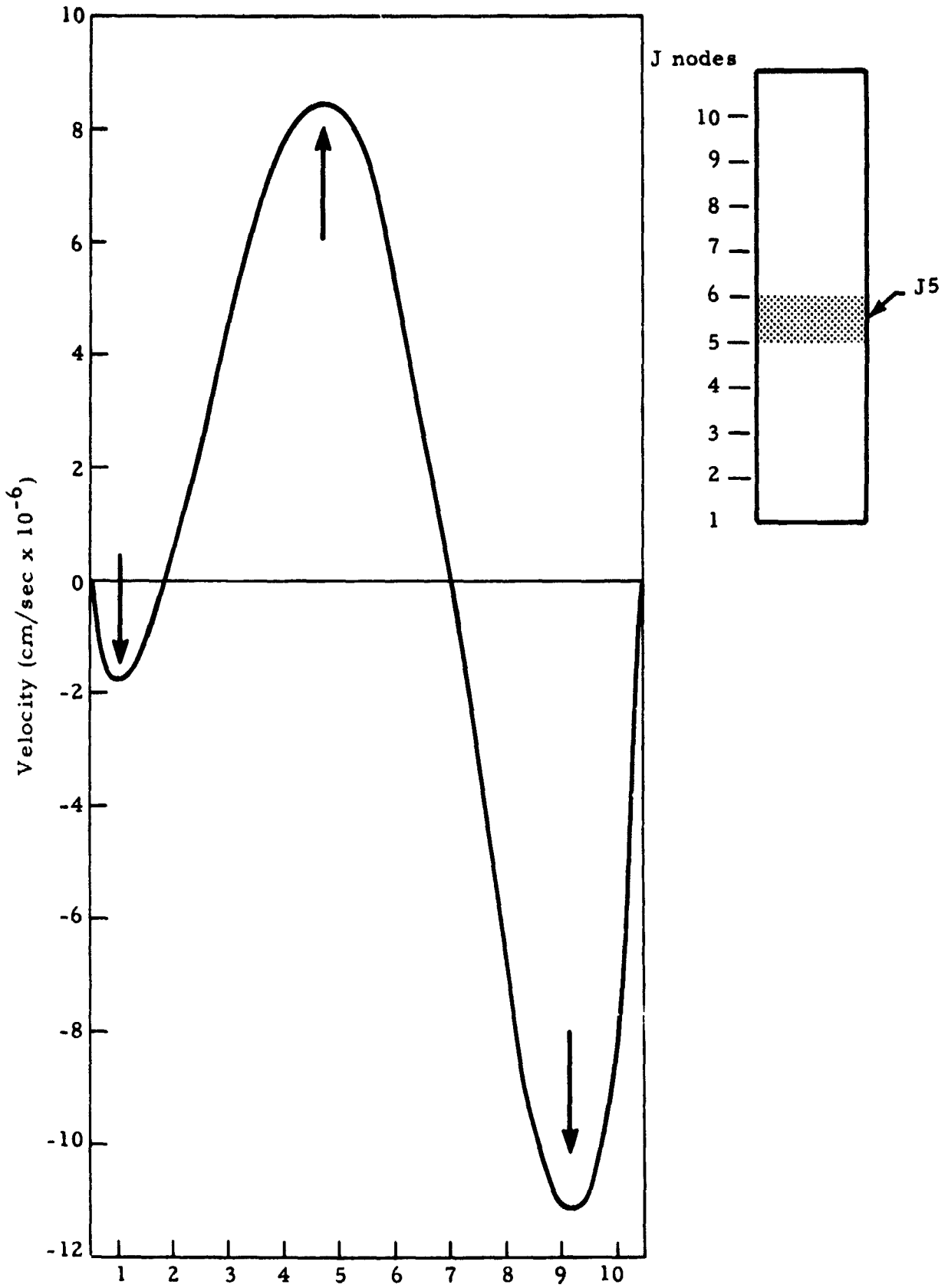


Fig. 15 - Velocity Profile in Rocket Cell at One Instant, 10<sup>-5</sup>g

## 5. DISCUSSION

Utilizing the crystallization of ammonium chloride from aqueous solutions as a model for the solidification behavior of metal alloys in any given circumstance requires a comparison of the following factors as a function of time:

- Convective flow velocities
- Convective flow patterns
- Temperature and concentration distributions
- Crystallization kinetics

The convective flow velocities are of interest in ingot crystallization because they conceivably could bend or break off delicate dendrite arms or cause various segregation phenomena. The question of how high a velocity can be tolerated before bending or breakage occurs has been only briefly addressed in past studies. Tiller and O'Hara<sup>(5)</sup> estimate that velocities of  $10\text{-}10^2$  cm/sec are required to elastically buckle a metallic dendrite raft whose stem is 50 to 100 times longer than it is thick. Somewhat smaller values are expected for deformation by yield. Further information on the criterion for dendrite arm breakage, however, was not found. It would not appear likely that the velocities of  $10^{-4}$  cm/sec and lower calculated in the present study would be sufficient to break off metallic dendrite arms. Velocities of  $10^{-4}$  cm/sec would be too low to break off ammonium chloride arms even though ammonium chloride crystals are more brittle than metallic crystals. The problem requires further study, but this study is inclined to discount velocities of  $10^{-4}$  cm/sec and lower as causing any dendrite arm breakage.

Convective flow velocities of about  $10^{-4}$  cm/sec can cause a variety of segregation behaviors.<sup>(6, 7)</sup> The  $10^{-4}$  cm/sec flow referred to in this

case is the interdendritic flow in the mushy liquid-solid region caused by solidification shrinkage or expansion with some contribution from gravity acting on density variations. Vigorous stirring of the bulk liquid, however, was found to be relatively ineffective in producing microsegregation in the presence of a metallic dendritic array.<sup>(8)</sup> The bulk convection velocities of  $10^{-4}$  to  $10^{-5}$  cm/sec calculated in the present study, therefore, can be discounted as having any significant effect on the crystallization processes. The reduction of gravity level undoubtedly reduced also the interdendritic fluid velocities.

As discussed in the preceding section, the calculated convective flow velocities were in the range of  $10^{-4}$  to  $10^{-5}$  cm/sec for the ammonium chloride cases and  $10^{-5}$  cm/sec or lower for the metal cases. In reality the velocities in the actual experiment were probably even lower. The computer analysis does not consider coupling. The result of coupling would decrease convective velocities because thermal cooling of the wall would drive the convective flow downward, as shown in Fig. 16a, and dendrite crystallization, which depletes the solute concentration, would drive the convective flow upward, as shown in Fig. 16b. The result could vary from the situation shown in Fig. 16c to that shown in Fig. 16e. The exact flow pattern is irrelevant to the present study because the uncoupled velocities were so low. At higher velocities the coupling could be a possible source of shearing action.

The computer calculations do not consider the heat of crystallization. Liberation of substantial heats of crystallization would have the effect of reinforcing the upward flowing convective currents. At low-g this would not be expected to be a large effect. Substantial heat liberation on crystallization would be expected to reinforce remelting. However, because no remelting was observed in the low-g test, this effect can also be discounted.

We now turn our attention to theories of the columnar to equiaxed transition in metal that do not depend primarily on gravity-driven convection.

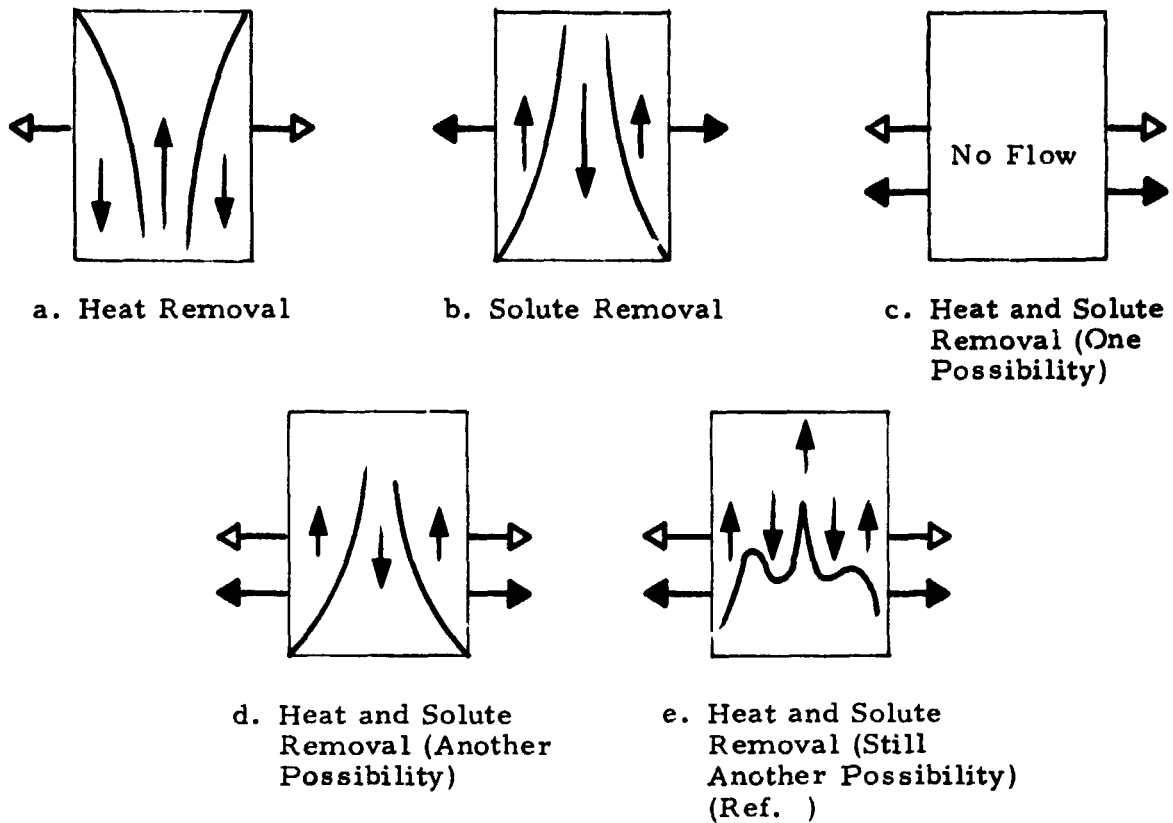


Fig. 16 - Schematic of Various Convections Driven by Thermal and Solutal Forces<sup>(9)</sup>

There are currently two of these, and we label them for discussion purposes as the Supercooling theory<sup>(10)</sup> and the Remelting theory.<sup>(11)</sup> The Supercooling theory holds that the transition occurs when constitutional supercooling occurs ahead of the solidifying interface — nucleation occurs in the supercooled region. In the Remelting theory, the small dendrite arms are melted off by thermal fluctuations arising either from a coupled interaction between diffusional mass and heat transport or thermal, convective oscillations. With the Supercooling theory convection is predicted to increase nucleation because convective mixing causes the liquidus temperature near the interface to increase. Convection would obviously also be predicted to increase equiaxed grains in the Remelting theory. In the Dendrite Remelting Rocket Experiment no new grains were observed ahead of the solidifying interface.

Tentatively therefore, the following conclusions are indicated: the Super-cooling theory is wrong and the Remelting theory is right with regard to convective thermal oscillations but not coupled diffusional transports. These conclusions, however, must be tested further with regard to what the thermal fields are under low-g and one-g conditions.

Two theories concerning solute macrosegregation are also candidates for low-g testing. One of these theories<sup>(12)</sup> maintains that interdendritic flow caused by solidification shrinkage is the cause of certain macrosegregation phenomena. The other theory<sup>(13)</sup> holds that another type segregation phenomenon is caused by a mechanism similar to that proposed in the Super-cooling theory. The results of the Dendrite Remelting Rocket Experiment would tend to refute the latter theory. Again, however, a definite conclusion awaits an assessment of the thermal fields.



## 6. CONCLUSIONS

Gravity-driven convective velocities were insignificant magnitudes during the Dendrite Remelting Rocket Experiment.

Gravity-driven convection would also be negligible in metallic systems under the same conditions.

The Dendrite Remelting Rocket Experiment, showing no secondary nucleation phenomena, indicates that Supercooling theories and Remelting theories (i.e., remelting by coupled diffusional transport) may not be applicable to ingot solidification. Definite conclusions, however, await a detailed analysis of the respective thermal fields involved in ammonium chloride and metallic systems.

More work is needed on how to match selected convection characteristics for both metallic systems and aqueous ammonium chloride systems. This will allow the aqueous solutions to be utilized more accurately as models or analogs for metallic systems.

## REFERENCES

1. Batchelor, G. K., "Heat Transfer by Free Convection Across a Closed Cavity Between Vertical Boundaries at Different Temperatures," Quart. Appl. Math., Vol. 12, 1959, p. 209.
2. Lindberg, W. R., and P. D. Haberstrah, "The Thermal-Burst Model of Thermohaline Natural Convection," AICHE Symp. Series 131, Vol. 69, C. Phillip Calver, editor, 1973.
3. Copley, S. M., A. F. Giamei, S. M. Johnson, and M. F. Hornbecker, "The Origin of Freckles in Unidirectionally Solidified Castings," Metall. Trans., Vol. 1, 1970, pp. 2193-2204.
4. Sharp, R. M., and Hellawell, A., "The Incidence of Convection During Solidification," J. Crystal Growth, Vol. 12, 1972, pp. 261-262.
5. Tiller, W. A., and S. O'Hara, "On the Mechanisms of Crystal Multiplication During Solidification in the Presence of Fluid Motion - Part 2," The Solidification of Metals, The Iron and Steel Institute, London, 1967.
6. Mehrabian, R., "Solidification Technology," Proceedings of the First Army Materials Technology Conference, Wentworth-by-the-Sea, Portsmouth, N. H., 22-25 October 1972.
7. Kaempffer, F., and F. Weinberg, "Interdendritic Fluid Flow in a Pb-Sn Alloy," Metall. Trans., Vol. 2, 1971, pp. 3051-3054.
8. Verhoeven, J., "Macrosegregation During Growth of a Dendrite Array into a Stirred Melt at Near Steady-State Conditions," Metall. Trans. AIME., Vol. 2, 1971, pp. 2673-2680.
9. Adams, J. A., and P. W. McFadden, "Simultaneous Heat and Mass Transfer in Free Convection with Opposing Body Forces," AICHE J., Vol. 12, 1966, pp. 642-647.
10. Winegard, W. C., and B. Chalmers, Trans. Am. Soc. Metals, Vol. 46, 1954.
11. Jackson, K. A., J. D. Hunt, D. R. Uhlmann and T. P. Seward, III, "On the Origin of the Equiaxed Zone in Castings," Trans. Met. Soc. AIME, Vol. 236, 1966, pp. 149-158.
12. Flemin, M. C., and G. E. Nereo, "Macrosegregation: Part 1," Trans. Metall. Soc. AIME, Vol. 239, 1967, pp. 1449-1461.
13. Ohno, A., "Compositional Depression of Undercooling and Formulation of Segregation Between Columnar and Equiaxed Crystal Zones," The Solidification of Metals, The Iron and Steel Institute, London, 1967, pp. 349-355.

Appendix A  
DYNAMIC AND THERMODYNAMIC SIMILITUDE  
OF GROUND AND FLIGHT EXPERIMENTS

## Appendix A

As discussed in the main body of the report, reduction of convective velocities is possible by decreasing (scaling) container dimensions, temperature differences or gravity levels. Convective velocities, however, are not the only parameters that need to be considered in scaling problems. Convective flow patterns and temperature/concentration distributions are also affected by a change of boundary conditions. For the case of ammonia chloride systems as analogues for metallic systems, it will probably not be possible to match every dependent phenomenon by a single change of boundary conditions, i.e., if we match the flow velocities, the flow patterns or the temperature profiles will probably be different. Insight into the reasons why an exact matching is probably not possible can be obtained from a consideration of a dimensionless analysis of the fluid flow equations. This is presented in the following paragraphs. The difficulties outlined in trying to match convective behaviors in two different type fluid systems with highly dissimilar thermal and transport properties highlights the advantages of having a well constructed computer program. With the aid of the computer the effects of a variety of boundary conditions can be quickly assessed. The matching or similitude problem then becomes a simple parametric study.

### ● THERMALLY DRIVEN CONVECTION SIMILITUDE ANALYSIS

For gaining some insight into scaling of ammonia chloride experiments to Pb-Sn in low-g flight, the following discussion is presented to help identify the important scaling parameters.

For simplicity, let us look at natural convection on a flat plate using an incompressible fluid at steady state. The governing equations become:

Mass

$$\frac{\partial u}{\partial x} + \frac{\partial v}{\partial y} = 0 \quad (1)$$

Momentum

$$\rho \left( u \frac{\partial u}{\partial x} + v \frac{\partial u}{\partial y} \right) = \rho g \beta (T - T_{\infty}) + \mu \frac{\partial^2 u}{\partial y^2} \quad (2)$$

Energy

$$\rho C_p \left( u \frac{\partial T}{\partial x} + v \frac{\partial T}{\partial y} \right) = k \frac{\partial^2 T}{\partial y^2} \quad (3)$$

Now for two systems (A and B) of incompressible fluid Eq. (1) will be exactly satisfied by simple scaling of the significant lengths and velocities. Let us now turn our attention to the momentum equation (Eq. (2)). For system A we can write Eq. (2) as follows:

$$\rho_A \left( u_A \frac{\partial u_A}{\partial x_A} + v_A \frac{\partial u_A}{\partial y_A} \right) = \rho_A g_A \beta_A (T - T_{\infty}) + \mu_A \frac{\partial^2 u_A}{\partial y_A^2} \quad (4)$$

Now let us consider another system B related to A by the following:

$$\begin{aligned} u_B &= C_v u_A & B_B &= C_B \beta_A \\ v_B &= C_v v_A & (T - T_{\infty})_B &= C_T (T - T_{\infty})_A \\ x_B &= C_L x_A & \mu_B &= C_{\mu} \mu_A \\ y_B &= C_L y_A & \rho_B &= C_{\rho} \rho_A \\ g_B &= C_g g_A \end{aligned} \quad (5)$$

We can write the equation of motion for system B in terms of quantities contained in system A

$$\frac{C_{\rho} C_v^2}{C_L} \left[ \rho_A \left( u_A \frac{\partial u_A}{\partial x_A} + v_A \frac{\partial u_A}{\partial y_A} \right) \right] = C_T C_{\rho} C_g C_{\beta} \left[ \rho_A g_A \beta_A (T - T_{\infty})_A \right] + \frac{C_{\mu} C_v}{C_L^2} \left[ \mu_A \frac{\partial^2 u_A}{\partial y_A^2} \right] \quad (6)$$

Now the momentum equation for system A (Eq. (4)) is identical to the momentum equation for system B (Eq. (6)) if the coefficients of the square bracketed terms are equal, i.e.,

$$\frac{C_{\rho} C_v^2}{C_L} = C_T C_{\rho} C_g C_{\beta} = \frac{C_{\mu} C_v}{C_L^2} \quad (7)$$

We can now substitute the physical quantities (Eq. (5)) into Eq. (7) to obtain the following, substituting  $V$  and  $L$  for significant velocity and length respectively:

$$\frac{\rho_B v_B^2 / L_B}{\rho_A v_A^2 / L_A} = \frac{\rho_B g_B \beta_B (T - T_{\infty})_B}{\rho_A g_A \beta_A (T - T_{\infty})_A} = \frac{\mu_B v_B / L_B^2}{\mu_A v_A / L_A^2} \quad (8)$$

If we combine the first and last terms we find that:

$$\frac{\rho_B v_B L_B}{\mu_B} = \frac{\rho_A v_A L_A}{\mu_A} \quad (9)$$

which says that the Reynolds number of system A and system B must be equivalent.

Now combining the second and third terms of Eq. (8) we find that

$$\frac{\rho_B g_B \beta_B (T - T_{\infty})_B L_B^2}{\mu_B v_B} = \frac{\rho_A g_A \beta_A (T - T_{\infty})_A L_A^2}{\mu_A v_A} \quad (10)$$

Since velocity is a dependent quantity we eliminate  $V_A$  and  $V_B$  using Eq. (9) and write

$$\frac{\rho_B^2 g_B \beta_B (T - T_\infty)_B L_B^3}{\mu_B^2} = \frac{\rho_A^2 g_A \beta_A (T - T_\infty)_A L_A^3}{\mu_A^2} \quad (11)$$

which states that the Grashof numbers of systems A and B must be equivalent. When buoyancy is the only driving force the fluid velocity is determined entirely by quantities within the Grashof number and Reynolds number equality is superfluous. Therefore, Grashof equality establishes dynamic similarity.

Now looking at the energy equation (Eq. (3)).

$$\rho C_p \left[ u \frac{\partial T}{\partial x} + v \frac{\partial T}{\partial y} \right] = k \left[ \frac{\partial^2 T}{\partial^2 y} \right] \quad (3)$$

and using the same logic just presented we will show that for similarity of temperature fields the Prandtl numbers ( $C_p \mu/k$ ) must be equal for dynamically similar systems A and B. Equating coefficients of the bracketed terms Eq. (3) in the manner presented for the momentum equations we find

$$\frac{C_\rho C_C C_T C_v}{C_L} = \frac{C_k C_T}{C_L^2} \quad (12)$$

Using the relationship of similar Reynolds numbers for dynamically similar flows (Eq. (9)) to eliminate  $C_v$ ,  $C_L$  and  $C_\rho$  dependence we find, after substituting physical quantities that;

$$\frac{C_{pB} \mu_B}{k_B} = \frac{C_{pA} \mu_A}{k_A} \quad (13)$$

which says that for similar temperature fields in dynamically similar flow fields we require equal Prandtl numbers.

Now since the solutions to the governing differential equations are identical for systems A and B if we have equivalent Grashof and Prandtl numbers, the Nusselt numbers will be equal and that the magnitude of the Nusselt number is only a function of these two quantities, i.e.,

$$\text{Nu} = \phi(\text{Gr}) \psi(\text{Pr}) . \quad (14)$$

Since the dynamics of the flow are determined by buoyancy forces which, in turn, are determined by density changes due to temperature gradients the amount of heat transfer (Nusselt number) is the driving parameter of the free convection problem.

If we return to Eq. (7) in our discussion

$$\frac{C_p C_v^2}{C_L} = C_T C_\rho C_g C_\beta = \frac{C_\mu C_v}{C_L^2} \quad (7)$$

we find that the first term is the coefficient to the inertia forces, the second to the buoyancy forces and the third to the viscous forces.

If we have a case where the inertia forces are small when compared with the viscous forces and the buoyancy forces, we can make the following similarity statement by neglecting the inertia term.

$$C_\rho C_g C_\beta C_T = \frac{C_\mu C_v}{C_L^2} \quad (15)$$

Now by making the substitutions (Eq. (5)) we find that

$$\left. \frac{C_p \rho^2 g \beta (T - T_\infty) L^3}{\mu k} \right|_B = \left. \frac{C_p \rho^2 g \beta (T - T_\infty) L^3}{\mu k} \right|_A \quad (16)$$

which is the Rayleigh number ( $\text{Pr} \cdot \text{Gr}$ ).



Now in this case, the heat transfer,  $Nu$ , can be defined as only a function of this parameter since it completely defines the flow  $Nu = \phi(Gr \cdot Pr)$ . It must be kept in mind that this analysis is good for small inertial forces when compared with viscous and buoyant forces.

For the liquid metal case ( $Pr \simeq .01$ ) in space ( $10^{-4}$  to  $10^{-5}$  g) the viscous forces and buoyant forces are small and one cannot make the assumption that inertial forces are much much less than either of these two. Therefore, the equation

$$Nu = \varphi(Gr) \psi(Pr) \quad (14)$$

must be used to define the net heat transfer to the fluid.

The significance of this discussion is, that in order to simulate the liquid metal case in low  $g$ , the net heat transfer relation (Eq. (14)) must be taken into account to achieve similarity in the driving mechanisms. Therefore, one must match both Prandtl and Grashof numbers to give total similarity. An additional complication arises for the two-dimensional case since the aspect ratio  $L/h$  must also be equivalent for both cases to achieve similarity.

The discussion previously presented has shown that dynamic similarity (equivalent velocity fields) can be achieved by equal Grashof numbers for systems A and B. However, one must keep in mind that the Grashof number can be thought of as a "local" Grashof number, that is that it contains spatial dependence throughout the field. Therefore, if we have two systems, A and B, the "local" Grashof number for a low Prandtl number liquid, i.e., liquid metal, and high Prandtl number liquid will be markedly dissimilar since the thermal energy transport mechanisms of the two systems are completely different, conduction and convection, respectively. This is true even though one may compute equivalent Grashof numbers using cell wall temperatures. We can now see that the important parameters for dynamic similarity for the one-dimensional case are both the Prandtl and Grashof numbers.

For the two-dimensional case the added complication of the additional momentum equation and added terms to the vertical momentum and energy equation require that similarity exists between the aspect ratios of system A and system B.

To summarize this discussion we have found the following to be required for dynamic similarity of two thermally driven convection cells:

- For dynamic similarity one must have equivalent "local" Grashof numbers.
- For equivalent "local" Grashof numbers we must maintain similar temperature fields.
- To achieve similar temperature fields we must have equal Prandtl numbers in addition to the similar velocity field.
- For the two-dimensional case we must have equivalent aspect ratios.

Although all of the convective behaviors of a liquid metal flight experiment probably cannot be matched exactly with a non-metal model, one or another of the convection features probably can be matched with suitable scalings.